JGR Atmospheres

Key Points:

- El Niño-Southern Oscillation (ENSO) and sudden stratospheric warmings (SSWs) modulate the stratospheric polar vortex at different time-scales
- The main SSW precursor independently of the ENSO phase is associated with wave activity over Eurasia
- The anomalous Eurasian wave pattern can be dominated by different wave numbers depending on the ENSO phase

Correspondence to:
F. M. Palmeiro,
fm.palmeiro@meteo.ub.edu

On the Influence of ENSO on Sudden Stratospheric Warmings

F. M. Palmeiro[1,2] ⓘ, J. García-Serrano[1,3] ⓘ, P. Ruggieri[4,5] ⓘ, L. Batté[6] ⓘ, and S. Gualdi[5,7] ⓘ

[1]Group of Meteorology, Universitat de Barcelona (UB), Barcelona, Spain, [2]Dpto. Física de la Tierra y Astrofísica, Universidad Complutense de Madrid, Madrid, Spain, [3]Barcelona Supercomputing Center (BSC), Barcelona, Spain, [4]Dipartimento di Fisica e Astronomia, Università di Bologna, Bologna, Italy, [5]Fondazione Centro Euro-Mediterraneo sui Cambiamenti Climatici (CMCC), Bologna, Italy, [6]CNRM, Université de Toulouse, Météo-France, CNRS, Toulouse, France, [7]Istituto Nazionale di Geofisica e Vulcanologia, Bologna, Italy

Abstract Using the extended ERA5 reanalysis and three state-of-the-art models, this study explores how El Niño-Southern Oscillation (ENSO) can influence the total frequency, seasonal cycle and preconditioning of sudden stratospheric warmings (SSWs). Reanalysis data shows that in the last seven decades, winters with SSWs were more common than winters without, regardless El Niño (EN) or La Niña (LN) occurrence or the ENSO/SSW definitions. In agreement with previous studies, our models tend to simulate a linear ENSO-SSW relationship, with more SSWs for EN, around mid-winter (January–February) as in reanalysis, and less for LN when compared to neutral conditions. Independently of ENSO, the main tropospheric precursor of SSWs appears to be an anomalous wave-like pattern over Eurasia, but it is dominated by wavenumber 1 (WN1) for EN and shows an enhanced wavenumber 2 (WN2) for LN. The differences in this Eurasian wave pattern, which is largely internally generated, emerge from the distinct configuration of the background, stationary wave pattern induced by ENSO in the North Pacific, favoring a stronger WN1 (WN2) component during EN (LN). Our results suggest that the ENSO-forced signal relies on modulating the seasonal-mean polar vortex strength, becoming weaker and more displaced (stronger and more stable) for EN (LN), while ENSO-unforced wave activity represents the ultimate trigger of SSWs. This supports the view that ENSO and SSWs are distinct sources of variability of the winter atmospheric circulation operating at different time-scales and may reconcile previous findings in this context.

Plain Language Summary Sudden stratospheric warmings (SSWs) are extreme events of the stratospheric polar vortex that consist in its deceleration and breakdown for several days, with implications on surface weather for several weeks. On the other hand, the atmospheric response to El Niño-Southern Oscillation (ENSO) has been shown to weaken the stratospheric polar vortex during El Niño and strengthen it during La Niña winters, and hence, potential modulation of the occurrence of SSWs by ENSO is expected. Reanalysis data shows that in the last seven decades, winters with SSWs were more frequent than winters without regardless of ENSO, and instead of having an impact on the SSW total frequency, El Niño seems to favor events in mid-winter (January–February). The main mechanism driving SSWs is thought to be anomalous upward wave activity from the troposphere into the stratosphere, reaching and perturbing the polar vortex. Independently of the ENSO phase, enhanced wave activity before SSWs is here found over Eurasia, thus pointing to this region as the main precursor of SSWs. While ENSO modulates the polar vortex at monthly/seasonal time-scales, SSWs do so at daily/weekly time-scales, representing distinct sources of variability of the polar vortex.

1. Introduction

The impact of El Niño-Southern Oscillation (ENSO) on the seasonal-mean state of the boreal winter stratosphere is relatively well accepted (see Domeisen et al., 2019 for a review). During El Niño (EN) winters, a weakening of the polar vortex and a warming in the stratosphere is observed in reanalysis (e.g., Garfinkel & Hartmann, 2007; Van Loon and Labitzke, 1987) and models (e.g., Cagnazzo et al., 2009; García-Herrera et al., 2006; Sassi et al., 2004). On the contrary, La Niña (LN) winters are associated with a strengthening and cooling of the stratospheric polar vortex (Hardiman et al., 2019; Iza et al., 2016; Manzini et al., 2006). This *canonical* signal is also captured at monthly time-scales, but it can be enhanced for EN and reduced for LN if a sudden stratospheric warming (SSW) occurs. Major SSWs are rapid disruption events, mainly occurring in the Northern Hemisphere, that imply a strong decay of the polar vortex strength with a consequent explosive warming in

the polar stratosphere (Matsuno, 1971). Although the influence of SSWs can persist several weeks in the lower stratosphere influencing surface weather/climate (Baldwin & Dunkerton, 2001; Charlton-Perez et al., 2013), their impact on the middle stratosphere reduces to some days, that is, the time needed for the polar vortex to recover (Limpasuvan et al., 2004). Thus, distinct from the ENSO impact on the seasonal-mean stratosphere, the life cycle of SSWs operates from daily to weekly time-scales. Because SSWs are extreme states of the polar vortex with the same sign as the EN signature, it is expected that EN winters potentially increase SSW occurrence while a reduction is presumed for LN winters. This idea has been intensively addressed and updated in consecutive studies using reanalysis data but conclusions were not always consistent, evidencing the effect of sampling in the short observational record and other sources of uncertainty such as the reanalysis product (see Table 2, Trascasa-Castro et al., 2019) or how SSWs and ENSO are defined (Song & Son, 2018). Yet, there is certain evidence of more SSWs occurring during EN than neutral conditions, while results for LN are more controversial (e.g., Polvani et al., 2017). Considering the most up-to-date records, Domeisen et al. (2019) concluded that SSW occurrence is favored during both phases of ENSO, but Song and Son (2018) showed that the LN effect on SSWs is not statistically significant, and using 65°N for detection instead of 60°N, SSWs occur with the same frequency during LN and neutral winters. Likewise, while models tend to confirm the positive impact of EN on SSW frequency (C. J. Bell et al., 2009; Oehrlein et al., 2019), they show a different behavior for LN, usually contributing negatively to the frequency of SSWs or not having any influence (Domeisen et al., 2015; Garfinkel et al., 2012; Song & Son, 2018; Taguchi & Hartmann, 2006; Trascasa-Castro et al., 2019).

The accepted mechanism to explain the EN impact on SSWs consists in a deepening of the Aleutian Low by the SST-forced wavetrain that constructively interferes with the climatological wave pattern, leading to positive eddy heat flux over this region and upward wave injection into the polar stratosphere (Garfinkel & Hartmann, 2008). While this mechanism would be consistent with an increased SSW frequency during EN, the SST-forced wavetrain is of opposite sign during LN and the Aleutian Low becomes weaker; hence, a different process might be at play to favor SSWs during LN. Using reanalysis and models, Garfinkel et al. (2012) suggested that the precursor region of SSWs is actually located in the northernmost part of the Bering Sea, surrounding the Russian Coast, and that this region is influenced by negative geopotential height anomalies during both ENSO phases. However, it does not reconcile how LN can strengthen the polar vortex and trigger SSWs simultaneously. Another ENSO impact on SSWs may involve the modulation of their precursors. Using reanalysis data, Barriopedro and Calvo (2014) found that SSWs occurring during EN (LN) are preceded by Atlantic and European (Pacific and Siberian) blocking that enhance different wavenumbers (WNs). This was in agreement with the modeling conclusions from Taguchi and Hartmann (2006) showing a preference for WN1 (WN2) amplification during EN (LN).

Timing is a potential issue in the ENSO-SSW relationship that has not yet been fully considered. Van Loon and Labitzke (1987) already noted that the ENSO signal on the stratosphere does not develop until January, and more recent studies show that the strongest stratospheric response to EN establishes by January (Ineson & Scaife, 2009; Manzini et al., 2006), concurrent with the full development of the tropospheric wavetrain in mid-winter (Bladé et al., 2008; King et al., 2018). Since SSW occurrence is associated with strong upward wave activity from the upper troposphere/lower stratosphere, modulating the seasonal cycle of this quantity may also alter the seasonal cycle of SSWs. In fact, Palmeiro et al. (2020) have shown a clear link between the intra-seasonal evolution of the meridional eddy heat flux at 100 hPa and SSW frequency.

The aim of this study is to differentiate the SST-forced response of the stratospheric polar vortex from internal variability, in order to identify the ENSO-related influence on the frequency, timing and tropospheric precursor structure of SSWs. To isolate the ENSO signal, a multi-model set of atmosphere-only sensitive experiments with prescribed ENSO-like SST patterns will be used, in addition to reanalysis data. Note that our multi-model approach is a novelty in this framework (cf. C. J. Bell et al., 2009; Taguchi & Hartmann, 2006; Trascasa-Castro et al., 2019) and provides an added value for robustness.

2. Data and Methodology

The fifth generation ECMWF atmospheric reanalysis (ERA5; B. Bell et al., 2021; Hersbach et al., 2020) covering 71 winters from 1950/1951 to 2020/2021 is used. Note that the date of SSWs in ERA5 has not yet been reported elsewhere (see Table 1), thus providing a novelty for the community, completing the SSW compendium (Butler et al., 2017) and results in Domeisen et al. (2019), their Table 1. In addition, three state-of-the-art atmosphere models contributing to the multi-model ensemble of the ERA4CS-funded MEDSCOPE project are employed:

Table 1
Sudden Stratospheric Warmings Dates Using U5570, U60 and the Corresponding ENSO Phase

Winter	SSW (U5570)	SSW (U60)	ENSO phase
1950/1951	22 December 1950; 27 January 1951	09 February 1951	NEU/NEU05
1951/1952	08 February 1952	18 February 1952	NEU/EN05
1952/1953	11 November 1952; 17 January 1953	19 November 1952	NEU/NEU05
1953/1954	–	–	NEU/EN05
1954/1955	10 January 1955	12 January 1955	NEU/LN05
1955/1956	–	–	LN
1956/1957	04 February 1957	04 February 1957	NEU/NEU05
1957/1958	27 January 1958	07 February 1958	EN
1958/1959	–	–	EN
1959/1960	10 January 1960	17 January 1960	NEU/NEU05
1960/1961	–	–	NEU/NEU05
1961/1962	–	–	NEU/NEU05
1962/1963	25 January 1963	26 January 1963	NEU/NEU05
1963/1964	–	–	EN
1964/1965	–	–	NEU/LN05
1965/1966	01 December 1965; 18 February 1966	16 December 1965; 22 February 1966	EN
1966/1967	–	–	NEU/NEU05
1967/1968	06 January 1968	07 January 1968	NEU/NEU05
1968/1969	24 November 1968; 12 March 1969	28 November 1968; 13 March 1969	EN
1969/1970	01 January 1970	01 January 1970	NEU/EN05
1970/1971	12 January 1971; 16 March 1971	18 January 1971; 19 March 1971	LN
1971/1972	–	–	NEU/LN05
1972/1973	30 January 1973	31 January 1973	EN
1973/1974	–	–	LN
1974/1975	–	–	NEU/LN05
1975/1976	–	–	LN
1976/1977	22 November 1976; 25 December 1976	09 January 1977	NEU/EN05
1977/1978	–	–	NEU/EN05
1978/1979	05 December 1978; 25 January 1979; 21 Feb 1979	22 February 1979	NEU/NEU05
1979/1980	–	01 March 1980	NEU/EN05
1980/1981	05 February 1981	04 March 1981	NEU/NEU05
1981/1982	03 December 1981	04 December 1981	NEU/NEU05
1982/1983	–	–	EN
1983/1984	21 February 1984	23 February 1984	NEU/LN05
1984/1985	29 December 1984	31 December 1984	LN
1985/1986	–	–	NEU/NEU05
1986/1987	22 January 1987	22 January 1987	EN
1987/1988	06 December 1987	07 December 1987; 14 March 1988	NEU/EN05
1988/1989	17 February 1989	21 February 1989	LN
1989/1990	–	–	NEU/NEU05
1990/1991	02 February 1991	–	NEU/NEU05
1991/1992	–	–	EN
1992/1993	–	–	NEU/NEU05

Table 1
Continued

Winter	SSW (U5570)	SSW (U60)	ENSO phase
1993/1994	01 January 1994	–	NEU/NEU05
1994/1995	22 January 1995	–	EN
1995/1996	–	–	NEU/LN05
1996/1997	22 November 1996	–	NEU/NEU05
1997/1998	27 December 1997	–	EN
1998/1999	15 December 1998; 25 February 1999	15 December 1998; 25 February 1999	LN
1999/2000	–	–	LN
2000/2001	21 November 2000; 01 February 2001	11 February 2001	NEU/LN05
2001/2002	26 December 2001; 16 February 2002; 26 March 2002	30 December 2001; 17 February 2002	NEU/NEU05
2002/2003	17 January 2003; 17 February 2003	18 January 2003	NEU/EN05
2003/2004	02 January 2004	05 January 2004	NEU/NEU05
2004/2005	–	–	NEU/EN05
2005/2006	12 January 2006	20 January 2006	NEU/LN05
2006/2007	22 February 2007	24 February 2007	NEU/EN05
2007/2008	21 February 2008	22 February 2008	LN
2008/2009	23 January 2009	24 January 2009	NEU/LN05
2009/2010	24 January 2010	09 February 2010; 23 March 2010	EN
2010/2011	–	–	LN
2011/2012	14 January 2012; 4 February 2012	–	NEU/LN05
2012/2013	04 December 2012; 05 January 2013	06 January 2013	NEU/NEU05
2013/2014	–	–	NEU/NEU05
2014/2015	04 January 2015	–	NEU/EN05
2015/2016	–	–	EN
2016/2017	23 November 2016; 01 February 2017; 25 February 2017	–	NEU/NEU05
2017/2018	11 February 2018	11 February 2018	NEU/LN05
2018/2019	30 December 2018	01 January 2019	NEU/EN05
2019/2020	–	–	NEU/NEU05
2020/2021	03 January 2021; 29 January 2021	04 January 2021	LN
ALL	8.9	6.3	
NEU/NEU05	9.2/10	5.8/5.0	
EN/EN05	8.3/8.0	7.5/7.2	
LN/LN05	8.2/8.8	7.2/6.7	

Note. Black, red, and blue colors stand for neutral, El Niño and La Niña conditions, respectively. Note that the decadal frequencies reported below are not statistically different between ENSO phases regardless of the ENSO/SSW definition according to a *t*-test at 95% confidence level.

the European Consortium EC-EARTH version 3.2 (Davini et al., 2017), whose atmospheric component is the ECMWF Integrated Forecasting System (IFS) cycle 36r4 with a horizontal resolution of ~80 km and 91 vertical levels up to 0.01 hPa; CNRM-CM6-1 (Roehrig et al., 2020; Voldoire et al., 2019), here referred to as CNRM, that includes ARPEGE-Climat version 6.3 as atmospheric component with ~100 km horizontal resolution and top at 0.01 hPa with 91 vertical levels; and, CMCC-SPS3 (Sanna et al., 2017), hereinafter CMCC, that uses CAM version 5.3 as atmospheric component with ~110 km horizontal resolution and 46 vertical levels up to 0.3 hPa. All experiments have fixed radiative forcing to year 2000 (present-day conditions) and HadISST2.2 (Titchner & Rayner, 2014) has been used to produce the boundary conditions. Three experiments of 50 ensemble members each have been performed: a control simulation (CTL) prescribing climatological SST computed over

1981–2010, and El Niño (EN) and La Niña (LN) experiments superimposing SST anomalies upon the climatology, built using linear regression of detrended monthly SST anomalies onto the winter (DJF) Niño3.4 index and amplified to reach a maximum of ±2.7°C during DJF similar to Taguchi and Hartmann (2006). The same patterns but with opposite sign are imposed for EN and LN, and restricted to 20°S–20°N. These SST anomalies, prescribed for a complete ENSO cycle from 1st June (year 0) to 31st May (year 1), are representative of strong canonical, eastern Pacific EN/LN episodes. Further details of the experimental set-up can be found in Mezzina, Garcia-Serrano, et al. (2022).

SSWs are detected when the zonal-mean zonal wind at 10 hPa becomes easterly at any latitude within the range 55–70 N (U5570; Palmeiro et al., 2015) to maximize SSW properties (Butler & Gerber, 2018) and to avoid possible biases in the stratospheric polar vortex edge. Events are separated with at least 21 days of westerlies and every winter's last wind reversal (i.e., the final warming), marking the transition to the summer circulation, is discarded. For a fair comparison to previous studies, when reporting SSW frequency, the traditional SSW definition considering zonal-mean zonal wind at 60N has been also used (U60; Charlton & Polvani, 2007). The observed ENSO events are selected from Table 1 in Domeisen et al. (2019) that considers the December-January-February Oceanic Niño Index (ONI). A comparison of results using strong events with a threshold of ±1 SD (standard deviation) or including also moderate events with ±0.5 SD (as in Domeisen et al. (2019)) is included in some parts of the analysis, namely EN/LN (strong) or EN05/LN05 (strong + moderate). Neutral winters are defined as those not classified as El Niño or La Niña (NEU and NEU05).

Daily fields of meridional wind (v) and temperature (T) are used to compute the meridional eddy heat flux in the lower stratosphere ($v*T*$ at 100 hPa), where the asterisks denote departures from the zonal mean. This is used as a measure of vertical wave propagation, sometimes referred to as wave injection, being proportional to the vertical component of the conventional Eliassen-Palm flux (e.g., Nishii et al., 2009).

To extract the ensemble-mean response to ENSO, namely the ENSO-forced response, differences EN-CTL and LN-CTL are computed. To be comparable, a similar approach is followed for ERA5 by subtracting the composite of neutral winters from El Niño or La Niña composites. The different significance tests are reported in the figure captions.

3. Results

Table 1 shows the ENSO phase and the SSW dates of occurrence in the ERA5 record using two SSW definitions (see Section 2): U5570 (Palmeiro et al., 2015) and U60 (Charlton & Polvani, 2007), although the former will be our benchmark due to its dynamical benefits (Butler & Gerber, 2018; Palmeiro et al., 2015). The frequency in ALL winters over the 1950–2021 period is 8.9 SSWs per decade and it is relatively similar under neutral (NEU), El Niño (EN) or La Niña (LN) conditions (9.2, 8.3, and 8.2, respectively; see end of Table 1). These results remain to some extent when using the traditional U60 definition: the frequencies in ERA5 for ALL (NEU) winters, EN and LN are 6.3 (5.8), 7.5, and 7.2 SSWs per decade, respectively. However, while U5570 detects less SSWs during ENSO than neutral conditions, the opposite occurs for U60, being the ENSO impact on SSW frequency sensitive to the SSW definition, albeit not statistically significant. When a less restrictive definition of ENSO episodes is used (±0.5 SD), the relative frequencies for ENSO winters are almost unaffected, regardless the SSW definition, and are not statistically distinguishable. It follows that, based on a large sampling, the observed occurrence of SSWs is similar under EN and LN conditions, which is consistent with recent observational collections (Butler et al., 2017; Domeisen et al., 2019).

Figure 1a shows the intraseasonal distribution of SSW occurrence from November to March during ALL winters (black) and the subsets of El Niño (blue) and La Niña (red) in ERA5. Considering first ALL SSWs, they mostly occur from late December to February, similar to what would result by combining the "historical" (1958–1978) and the "comparison" (1979–2012) periods in Ayarzagüena et al. (2019) using the WMO definition (similar to U60). Interestingly, there is a peak of SSW occurrence in late January–early February during EN (solid red) and a minimum during LN (solid blue); although they are not significantly different. As described in Palmeiro et al. (2020), the seasonal cycle of the latitudinally integrated meridional eddy heat flux $v*T*$ at 100 hPa (see Section 2) can be used as a proxy for the wintertime distribution of SSWs, regardless the wave activity comes from the troposphere (as traditionally considered) or is partially triggered from the tropopause (Boljka & Birner, 2020). This analysis of $v*T*$ is based on daily means from the composited ENSO years, not on daily averages around
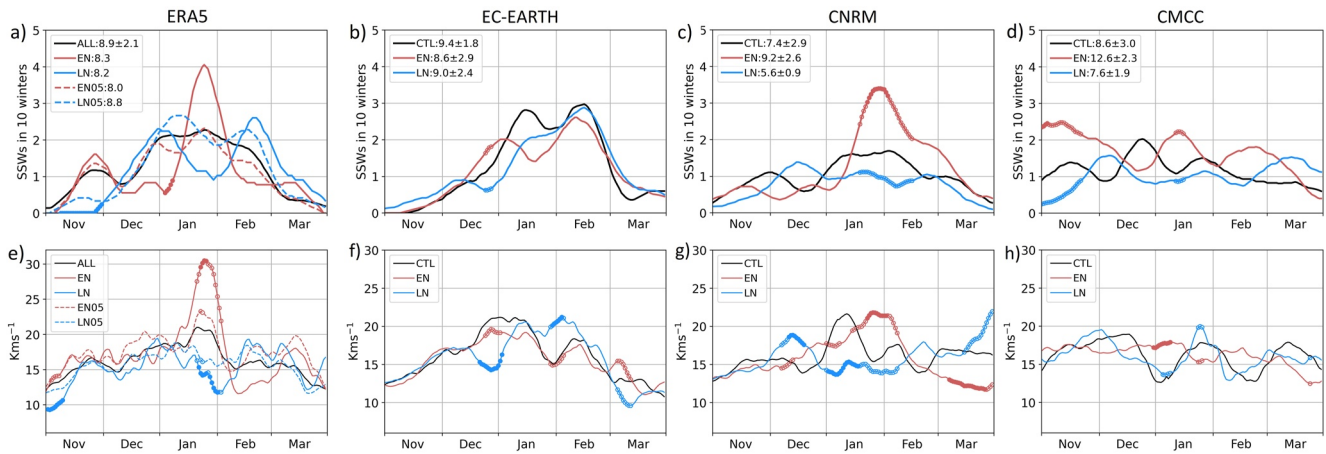
Figure 1. Seasonal distribution of (a–d) SSWs per decade, detected with U5570, in a [−10, 10]-day window around the SSW date and (e–h) daily mean of the meridional eddy heat flux ($v*T*$) zonally averaged over 60–75°N at 100 hPa for ALL (black), El Niño (red) and La Niña (blue) winters in ERA5. Filled (empty) circles in red and blue curves indicate statistically significant differences between ENSO (El Niño) and NEU (La Niña) at the 95% confidence level using a t-test. Time-series are smoothed with a 7-day running-mean. Numbers shown in the legend of the top panels indicate the decadal frequency and standard deviation of SSWs per winter; in ERA5 the standard deviation is estimated for ALL.

SSW dates. Comparison between Figures 1a and 1e confirms the relationship depicting maximum/minimum amplitude in mid-winter for EN/LN, respectively, which in this case are statistically distinguishable. Similar to the SSW distribution, the difference in $v*T*$ becomes more prominent for EN/LN (solid) as compared to EN05/LN05 (dashed).

To isolate the ENSO-forced potential effect on SSW frequency, three different experiments of 50 complete winters have been performed and analyzed (see Section 2): CTL, with prescribed climatological SST, and EN (LN) superimposing strong El Niño-(La Niña-)like SST anomalies in the tropical Pacific. In general, the models show SSW frequencies close to ERA5. In CTL, these are 9.4, 7.4, and 8.6 SSW per decade in EC-EARTH, CNRM and CMCC, respectively (cf. legends in Figure 1 and the U5570 column in Table 1 for NEU/NEU05). Although CNRM shows the lowest frequency, it depicts the most realistic intraseasonal distribution (cf. black lines in Figures 1a and 1c). The simulated SSW frequencies appear to be sensitive to ENSO, where the models show the typical, previously reported (e.g., Song & Son, 2018; Taguchi & Hartmann, 2006; Trascasa-Castro et al., 2019), linear relationship with fewer SSWs during LN and more SSWs during EN, particularly CNRM and CMCC. The exception is EC-EARTH for EN, showing a similar frequency to LN and less SSWs than CTL, which could be explained by the difficulty of the model to properly capture the El Niño teleconnection to the polar stratosphere (Mezzina, Garcia-Serrano, et al., 2022; Mezzina, Palmeiro, et al., 2022). CNRM is highly sensitive to EN and shows a strong peak of SSWs in late January–early February (Figure 1c), which is also consistent with a concomitant increase of $v*T*$ (Figure 1g) as seen for ERA5 (Figure 1, left column, red). To a lesser extent, the mid-winter peak is also reproduced by CMCC, displaying also more SSWs (Figure 1d) and significantly more wave injection (Figure 1h) than both CTL and LN. Note that its SSW difference in November is not found in reanalysis and could be related to model biases reported in Portal et al. (2022). EC-EARTH shows stronger wave activity (Figure 1f) and more SSWs in EN than in LN (Figure 1b) in late December–early January, but not distinguishable from CTL. Overall, with the exception of CNRM, the models do not correctly simulate the observed intraseasonal timing of SSWs and integrated eddy heat flux related to ENSO (Figure 1, left column). Notwithstanding, it is worth noting the consistent mirrored behavior of the SST-forced $v*T*$, particularly in the three models (Figure 1, bottom).

To further inspect the ENSO-forced signal, anomalies in the tropospheric circulation and wave injection are now considered for mid-winter (January–February), when the atmospheric response to ENSO is fully established (e.g., Toniazzo & Scaife, 2006; see also Section 1).

Figure 2 (top) shows the ensemble-mean response to EN in geopotential height at 500 hPa (Z500). The simulated patterns (Figures 2b–2d) rightly project on the observational composite (Figure 2a), all depicting the well-known extratropical response to El Niño, with a wavetrain signature that includes the deepening of the Aleutian Low (e.g., Trenberth et al., 1998). Associated with this anomalous, stationary wave-like pattern, the three models
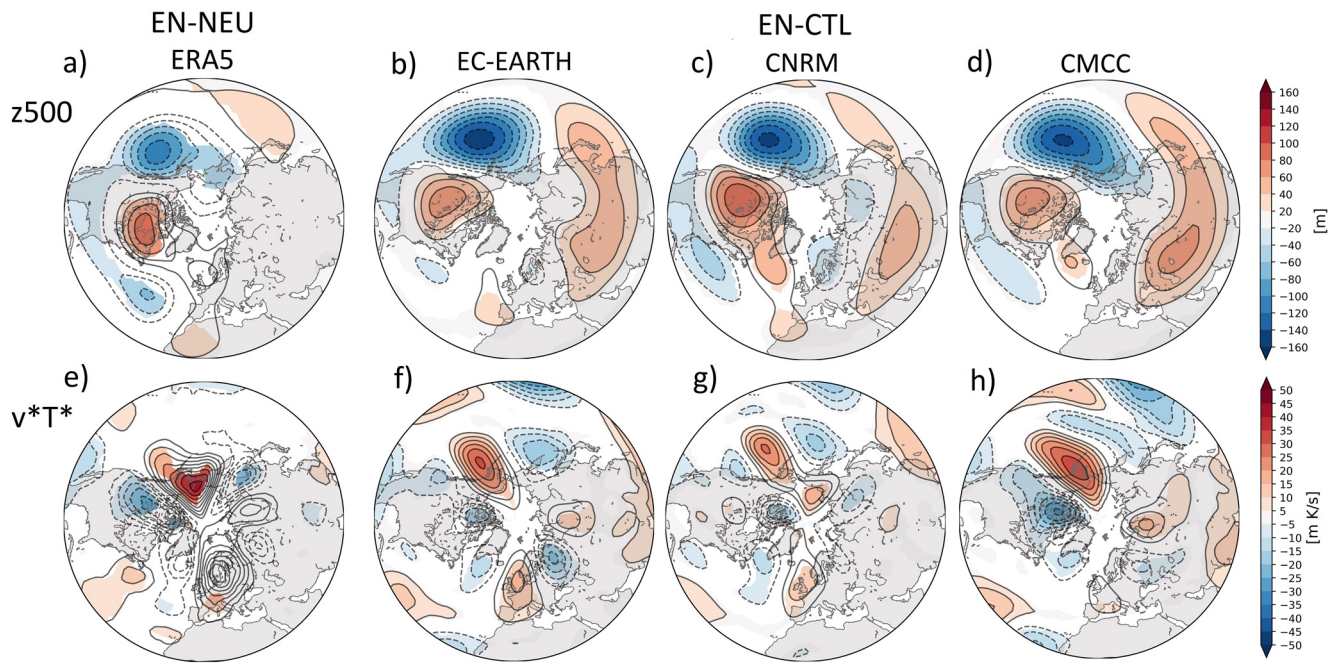
Figure 2. Anomalies of (top) geopotential height at 500 hPa and (bottom) meridional eddy heat flux (*v*T*) at 100 hPa for El Niño in January–February, computed as composite difference EN-NEU in ERA5 (left) and as ensemble-mean difference EN-CTL in the models (EC-EARTH, CNRM, CMCC). Statistically significant areas at 95% confidence level based on a two-tailed *t*-test for difference of means are shaded.

show a strengthening accompanied by an eastward shift of the climatological center of positive *v*T* over eastern Eurasia-western North Pacific (Newman & Nash, 2000), which leads to a dipole-like structure of *v*T* over the Aleutian Islands (Figures 2f–2h). This El Niño-forced dipolar anomaly in wave injection has been reported to be skilfully predicted by seasonal forecast systems (Portal et al., 2022) and linearly related to both the Niño3.4 index
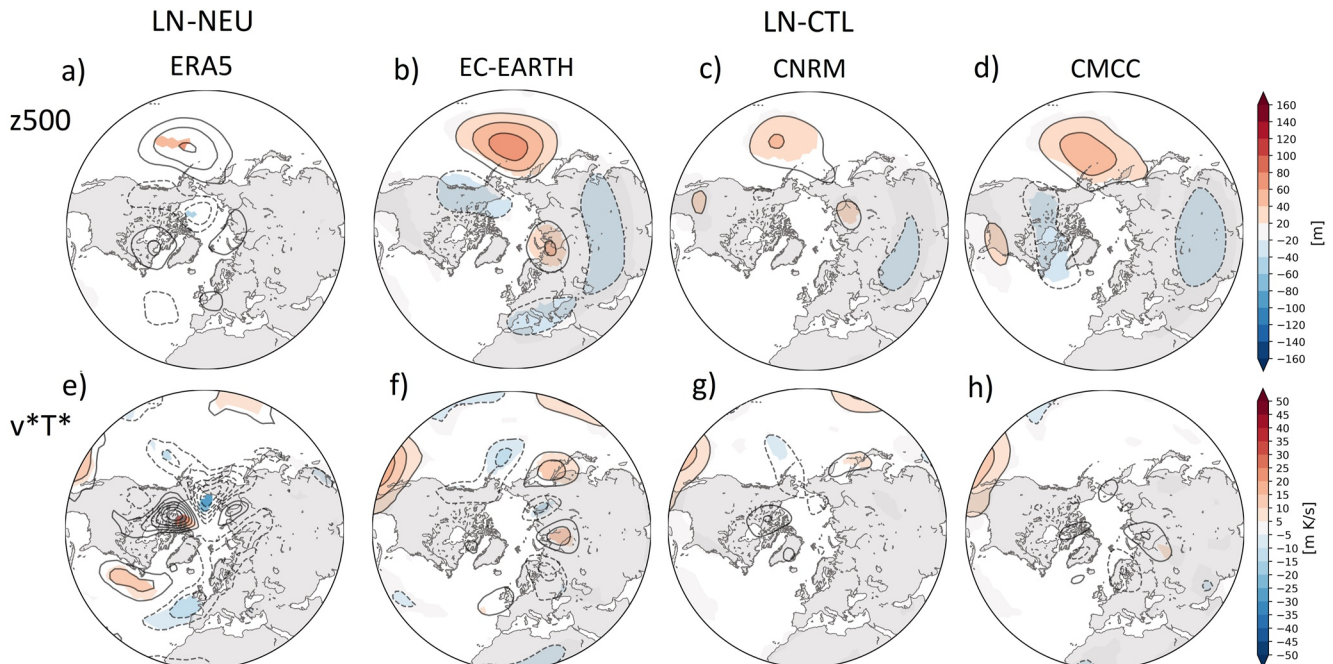

Figure 3. Same as Figure 2, but for La Niña.

(Portal et al., 2022) and the Pacific-North American pattern (Orsolini et al., 2009) in reanalysis. This anomalous wave injection is likely related to the El Niño perturbation of the polar vortex in the middle-upper stratosphere (e.g., Orsolini et al., 2008), namely the seasonal-mean weakening and displacement toward Scandinavia (see Figure 4). The stratospheric seasonal-mean response to ENSO in this set of experiments is extensively analyzed in Mezzina, Palmeiro, et al. (2022).

Similarly, Figure 3 (top) shows the expected Northern Hemisphere tropospheric response to La Niña, with a wave-train opposite in sign to that of El Niño (Figure 2, top), implying a weakening of the Aleutian Low. This anomalous wave-like pattern is weaker and shifted westward with respect to the extratropical response to EN in both ERA5 (Figure 3a) and the three models (Figures 3b–3d), in agreement with previous observational (e.g., Ayarzagüena et al., 2018; Deser et al., 2017) and modeling (e.g., Jiménez-Esteve & Domeisen, 2019; Trascasa-Castro et al., 2019) studies (see discussion in Mezzina, Garcia-Serrano, et al. (2022)). The ensemble-mean $v*T*$ (Figures 3f–3h) do not show any clear difference as compared to CTL, consistent with the results in Figure 1, although there are hints of negative anomalies as in ERA5 (Figure 3e), that is, suppression of wave activity over the eastern North Pacific, but weak and marginally significant. Even so, the three models yield a seasonal-mean state of the polar vortex that is colder and stronger than CTL (Mezzina, Palmeiro, et al., 2022; see Figure 4).

In order to explore the relationship between the SST-forced atmospheric response to ENSO (Figures 2 and 3) and the occurrence of SSWs (Figure 1), Figure 5 shows the composite of Z500 anomalies over the [−10, 0]-day period before SSWs in all events from ERA5 (Figure 5a) and the CTL simulations (Figures 5b–5d), and separately for EN/LN years (Figures 5e and 5i) and the sensitivity experiments (Figures 5f, 5g, 5h, 5j, 5k, and 5l). Most precursor patterns include or are dominated, in fact, by the same wave-like structure over Eurasia, which projects on the EU1 pattern (Barnston & Livezey, 1987) later identified as the Scandinavian pattern, that constitutes a prominent mode of internal variability associated with Rossby wave propagation dynamics and maintained by transient-eddy feedback (e.g., Bueh & Nakamura, 2007; Liu et al., 2014). This Eurasian wave pattern consists of a high-pressure system over Scandinavia and a low-pressure system downstream over Siberia (see Appendix A), extracting cold air from polar latitudes over central Eurasia and advecting warmer air from mid-latitudes over eastern Eurasia and the northern North Pacific. As a consequence, the Eurasian wave pattern shows positive eddy heat flux over the latter regions (Figure 6), constructively interfering with the two main climatological areas of wave injection at 100 hPa (e.g., Newman & Nash, 2000). Although part of this eddy heat flux could be associated with processes at the tropopause/lower stratosphere (Boljka
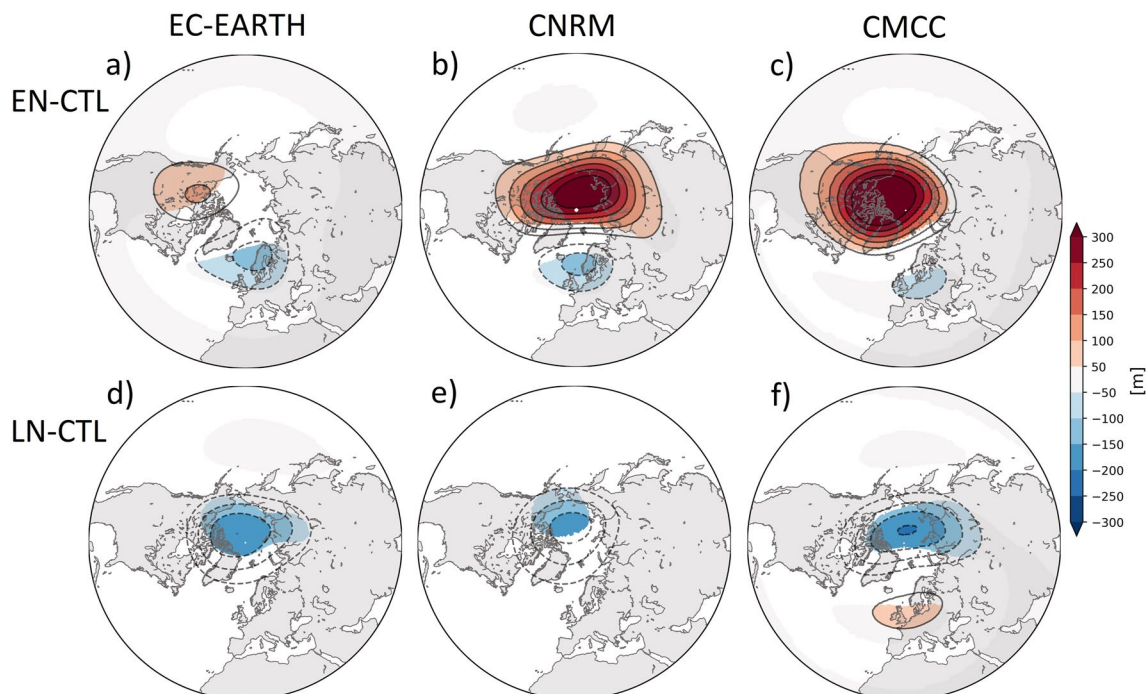

Figure 4. January–February ensemble-mean differences in geopotential height at 30 hPa for EN-CTL (top) and LN-CTL (bottom) in the models (EC-EARTH, CNRM, CMCC). Statistically significant areas at 95% confidence level based on a two-tailed t-test for difference of means are shaded.
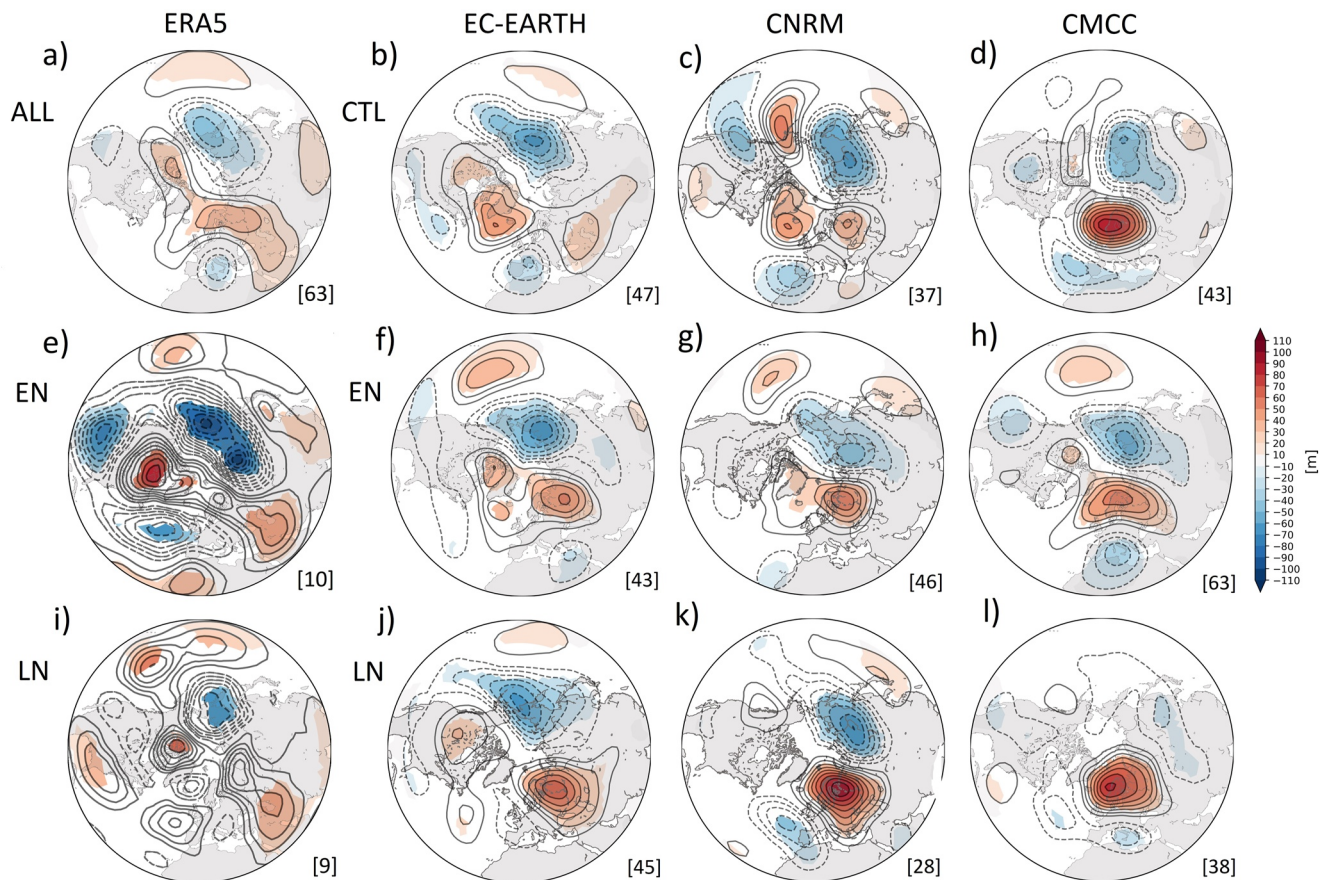
Figure 5. Anomalies of geopotential height at 500 hPa over the [−10, 0]-day period before SSWs in (from left to right) ERA5, EC-EARTH, CNRM, and CMCC for ALL/CTL (top), EN (middle) and LN (bottom). Statistically significant areas at 95% confidence level according to a 1,000-trial Monte Carlo test are shaded. Numbers in the bottom-right corner of each panel are the events included in the composite.

& Birner, 2020; de la Cámara et al., 2019), the anomalous wave-like pattern over Eurasia is indeed in phase with the two centers of action where climatological WN1 and WN2 coincide in sign (Garfinkel et al., 2010; see Figure 9 below). For CTL, in addition to the Eurasian wave pattern, the SSW precursors in EC-EARTH (Figure 5b) and CNRM (Figure 5c) include wave-like anomalies in the North Pacific-American sector and what probably is mixed with the SSW impact, a negative NAO-like anomaly in the Euro-Atlantic sector. In ERA5 (Figure 5a) and CMCC (Figure 5d), the Eurasian wave pattern is more isolated. For ENSO, the SSW precursory signals in ERA5 (Figures 5e and 5i) additionally show a distorted version of the large-scale wavetrain; but in general they are noisier. When the sampling is increased by considering also moderate events (EN05/LN05; Domeisen et al., 2019), the Eurasian wave pattern comes out more cleanly (Figures 7a and 7c). But interestingly, in the EN/LN experiments, where the ENSO forcing is prescribed, the three models consistently display the anomalous wave-like pattern over Eurasia as the most robust SSW precursor (Figures 5f, 5g, 5h, 5j, 5k, and 5l). These results suggest that the ENSO-forced atmospheric response (Figures 2 and 3) is not primarily responsible for the SSWs occurring under El Niño and La Niña conditions.

To gain understanding of the dynamics prior to SSWs, the precursors (Figures 5e–5l) are decomposed using zonal Fourier transform into WN1 (Figure 8, black contours) and WN2 (Figure 8, green contours), since there is the notion that the ENSO-SSW relationship is associated with an amplification of WN1 (WN2) during El Niño (La Niña) (see Section 1). In line with this, WN1 clearly dominates the Eurasian wave pattern for EN in the three models (Figures 8b–8d), while WN2 has a much larger amplitude, comparable to WN1, for LN (Figures 8f–8h). The results hold for ERA5 (Figures 8a and 8e), but the patterns are noisier (as in Figures 5e and 5i); again, EN05/LN05, with more sampling, smooth the signals (Figures 7b and 7d). The question that then emerges is how the same SSW precursor, that is, the anomalous wave-like pattern over Eurasia, considering it is internally generated and not forced by ENSO (cf. Figures 2, 3, and 5), can be modulated and project onto different WNs depending on the ENSO phase.
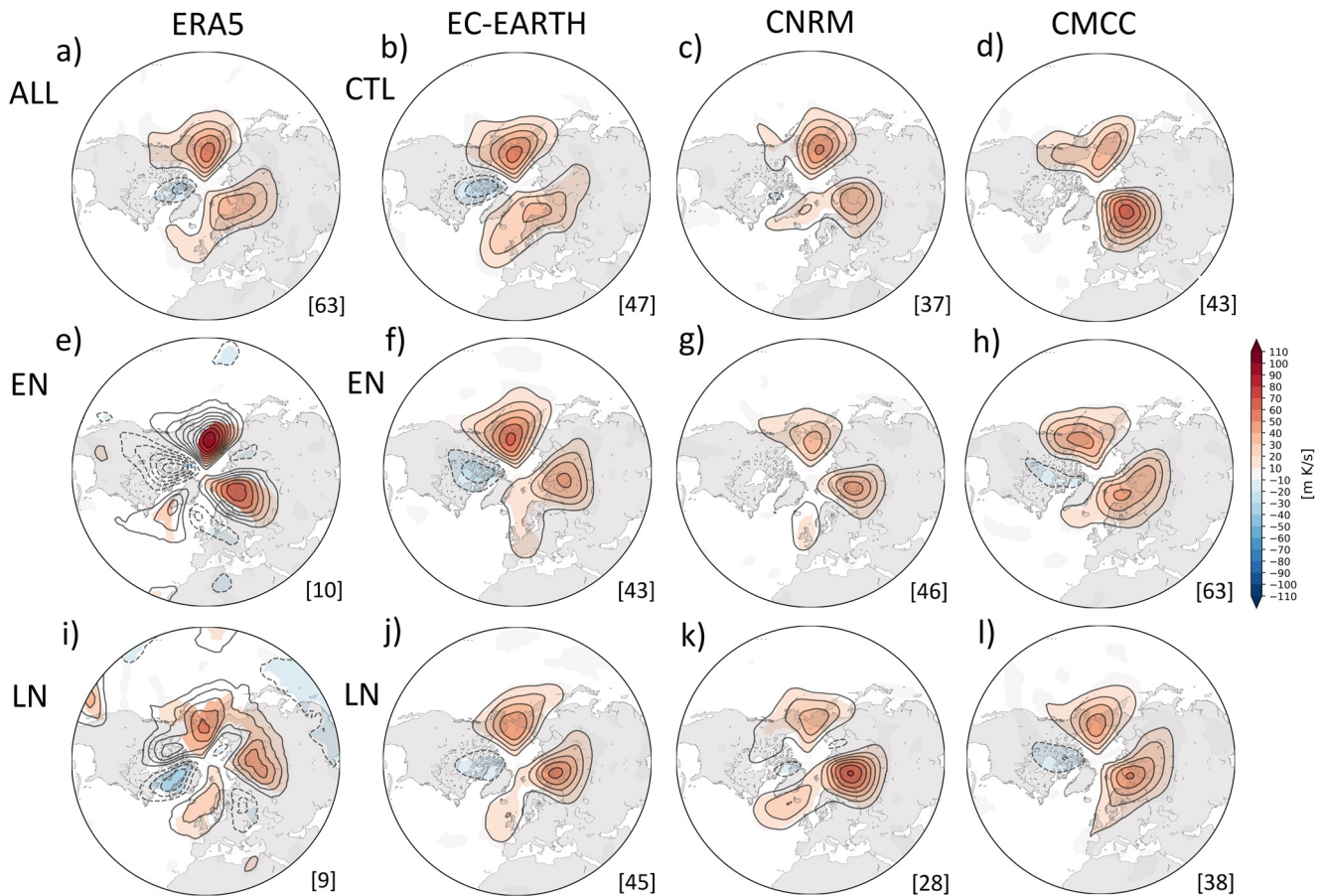
Figure 6. Same as Figure 5, but for the meridional eddy heat flux (v^*T^*) at 100 hPa.

Recall that the ENSO-forced atmospheric response does not show circulation anomalies over Eurasia. The hypothesis is that ENSO modifies the background wave pattern upon which the SSW-related anomalous wave pattern overlays.

Figure 9, first, displays the background, full stationary wave pattern (top) and its WN components (middle-bottom) from the ERA5 climatology and CTL experiments. Overall, the models properly simulate the stationary eddy structure, with small biases in the amplitude (Figures 9a–9d). The amplitude and location of the climatological WN1 are also well simulated (Figures 9e–9h), with the exception of CNRM (Figure 9g) that underestimates its magnitude at the expense of overestimating WN2 compared to the other models (Figure 9k). EC-EARTH (Figure 9j) and CMCC (Figure 9l) correctly simulate the climatological WN2 as compared to reanalysis (Figure 9i). On the other hand, as it is well known (see Domeisen et al., 2019 for review): El Niño tends to strengthen and expand the Aleutian Low, here illustrated with the full eddy-Z500 from the EN composite in ERA5 and the ensemble-mean of EN experiments (Figures 10a–10d, shading); while La Niña tends to weaken and contract the Aleutian Low, as shown in the LN composite and the ensemble-mean of LN experiments (Figures 10e–10h, shading). Note that these ENSO-forced circulation changes in the North Pacific are associated with the corresponding tropospheric wavetrain triggered from the tropical Pacific (Figures 2 and 3). More importantly, the El Niño-forced deepening of the Aleutian Low and anomalous cyclonic circulation over the eastern North Pacific lead the WN1 component of the stationary eddy (Figure 10 black contours) to have a ∼30% larger amplitude for EN (Figure 10, top) than LN (Figure 10, bottom). Arithmetically, the corresponding mirrored signature over western Eurasia also strengthens. Under La Niña conditions, the WN1 (black contours) and WN2 (green contours) components of the stationary wave pattern have comparable amplitude. Further, the La Niña-forced anomalous anticyclonic circulation over the eastern North Pacific shifts the WN2 component of the stationary eddy westward, namely clockwise, in LN (Figure 10, bottom) with respect to EN (Figure 10, top). Arithmetically, that shift leads to a stronger projection over eastern Eurasia (negatively) and Scandinavia (positively), although the amplitude is unaffected (see also Appendix A).
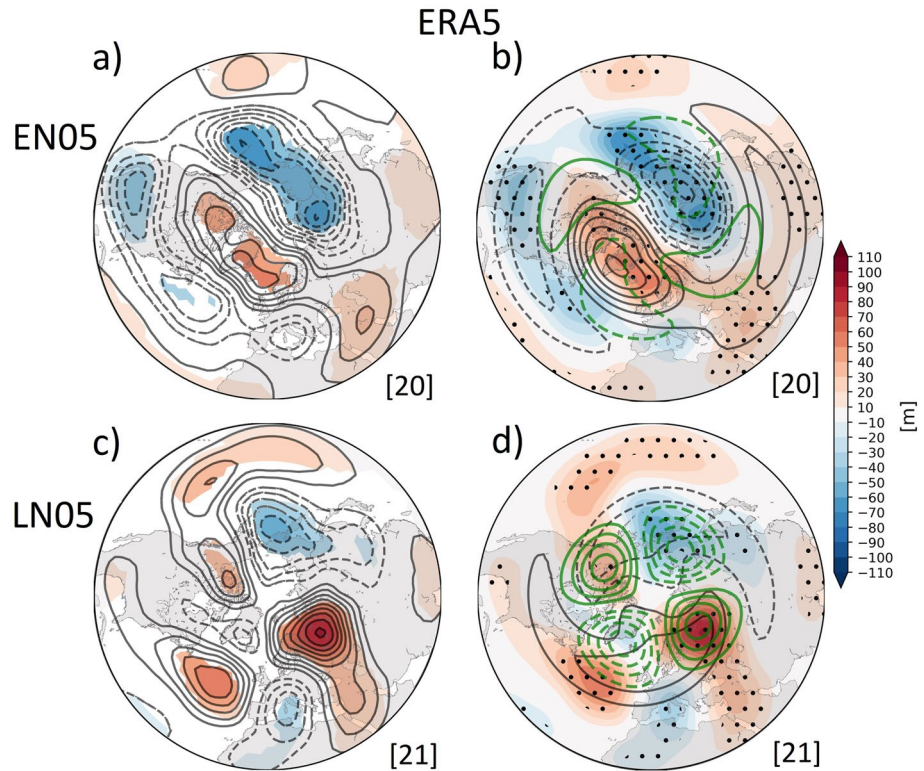
Figure 7. Anomalies of geopotential height at 500 hPa over the [−10, 0]-day period before SSWs in ERA5 for EN05 (top) and LN05 (bottom). (Left) same as in Figures 5e and 5i, but for EN05 (LN05). (Right), WN1 (black contours) and WN2 (green contours) components superimposed over the anomalies (shading). Note that contours in the left column correspond to the shading in the right column. Statistically significant areas at 95% confidence level according to a 1000-trial Monte Carlo test are shaded (dotted) in left (right) column.

In summary, the results suggest that there is no clear link between the wavetrain response to ENSO in the North Pacific and the dominant SSW precursor, that is, the Eurasian wave pattern (Figures 2–5); with the former being ENSO-forced and the latter internally generated. Thus, the ENSO-SSW relationship appears to be limited to a modulation of the seasonal-mean polar vortex state, whereas the occurrence of SSWs is largely triggered by ENSO-unrelated wave activity over Eurasia (Figures 5 and 6). Interestingly, the dominant SSW precursor has a stronger WN1 component during El Niño (Figure 8, top), and a strengthened amplitude of WN2 but similar to WN1 during La Niña (Figure 8, bottom). It is hypothesized that ENSO modifies the background, stationary wave pattern, via changes of the Aleutian Low, in a way that the anomalous Eurasian wave pattern projects differently depending on the ENSO phase.

4. Discussion and Conclusions

The ERA5 reanalysis and three state-of-the-art models, EC-EARTH, CNRM, and CMCC have been used to explore the ENSO modulation of SSW occurrence.

Results indicate that in the observational record, 1950–2021, winters with SSWs have been more frequent compared to winters without. This is particularly evident using a more general SSW definition (U5570, Palmeiro et al., 2015), which increases the sampling but maximizing the key properties of SSWs (Butler & Gerber, 2018), than the traditional U60 (Charlton & Polvani, 2007). Whether ENSO favors SSW occurrence as compared to neutral conditions (being less with U5570 and more with U60) depends on how SSWs are defined, but similar SSW frequencies are obtained for El Niño and La Niña regardless of the SSW definition. These results agree with previous studies considering a shorter period (1958–2017; e.g., Domeisen et al., 2019) also independently of the SST threshold (±1SD or ±0.5SD). Even so, considering the substantial uncertainty in the observational records (e.g., Butler & Polvani, 2011; Song & Son, 2018), this question remains unclear. In the sensitivity experiments,
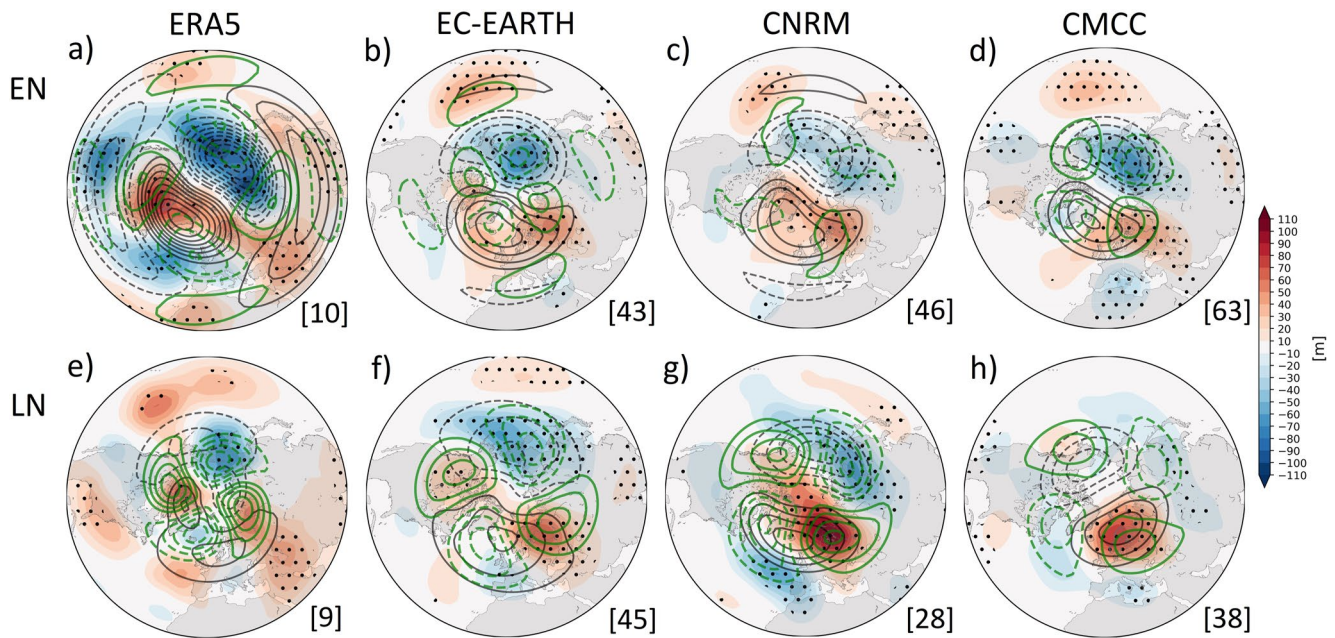
Figure 8. Same as Figure 7 (right) but in (from left to right) ERA5, EC-EARTH, CNRM, and CMCC for EN (top) and LN (bottom).

compared to CTL (with climatological SSTs), the models tend to show an increase of SSWs during EN and a decrease during LN although not statistically significant. This linear relationship between ENSO and SSWs has been typically found in climate models (Domeisen et al., 2015; Garfinkel et al., 2012; Polvani et al., 2017; Song & Son, 2018; Weinberger et al., 2019), and in similar atmosphere-only experiments to those described here prescribing ENSO forcings (Garfinkel et al., 2012; Taguchi & Hartmann, 2006; Trascasa-Castro et al., 2019) or only El Niño-like SST anomalies (C. J. Bell et al., 2009; Oehrlein et al., 2019). Nevertheless, caution is advised when comparing reanalysis with model outputs as the simulated/prescribed SST forcing may not represent the observed skewness of ENSO, particularly with respect to the amplitude of La Niña (e.g., Timmermann et al., 2018), but might in future climate (Hardiman et al., 2019).

Unlike the uncertain influence on the total SSW frequency, the intraseasonal distribution of SSWs in ERA5 suggests that ENSO can have an impact during mid-winter (January–February), which is not unexpected since the ENSO signal on the mean-state of the stratosphere reaches its maximum at this time of the year (Cagnazzo & Manzini, 2009; Ineson & Scaife, 2009; Manzini et al., 2006; Sassi et al., 2004; Van Loon and Labitzke, 1987). It is found that mid-winter SSWs have occurred more (less) frequently in EN (LN) years (using ±1 SD to define ENSO events; Figure 1a). ERA5 and the ensemble-mean response show significant eddy heat flux anomalies over the eastern North Pacific for EN (Figure 2), related to the Rossby wavetrain and the eastward shift of the climatological center of positive v^*T^* over the Aleutian Islands, in agreement with previous studies (e.g., Portal et al., 2022). The anomalies have opposite sign for LN (Figure 3), but the amplitude of z500 is much weaker and the statistical significance of v^*T^* is limited, also consistent with previous studies (e.g., Mezzina, Garcia-Serrano, et al., 2022; Mezzina, Palmeiro, et al., 2022).

On the other hand, the dominant precursor signal of SSWs in ERA5, CTL simulations, and particularly during observed EN/LN winters and in the EN/LN experiments, corresponds to a wave-like pattern over Eurasia (Figures 5 and 7) that strongly resembles the variability mode referred to as the Scandinavian pattern (e.g., Bueh & Nakamura, 2007; Liu et al., 2014). This Eurasian wave pattern has been consistently reported in previous studies as the primary SSW precursor (e.g., Cohen & Jones, 2011; Diaz-Durán et al., 2017; Hurwitz et al., 2012; Limpasuvan et al., 2004; Marshall & Scaife, 2010; Nakagawa & Yamazaki, 2006; Orsolini et al., 2011), as well as the tropospheric circulation preceding the NAO through a stratospheric pathway (e.g., García-Serrano et al., 2015, 2017; Kuroda & Kodera, 1999; Peings, 2019; Ruggieri et al., 2016, 2017; Takaya & Nakamura, 2008). Note that the cyclonic precursory signal over the western North Pacific reported by Garfinkel et al. (2012) could represent the downstream anomaly of the wave-like pattern over Siberia. The Eurasian wave pattern projects both onto the climatological WN1 and WN2 (Figure 9),
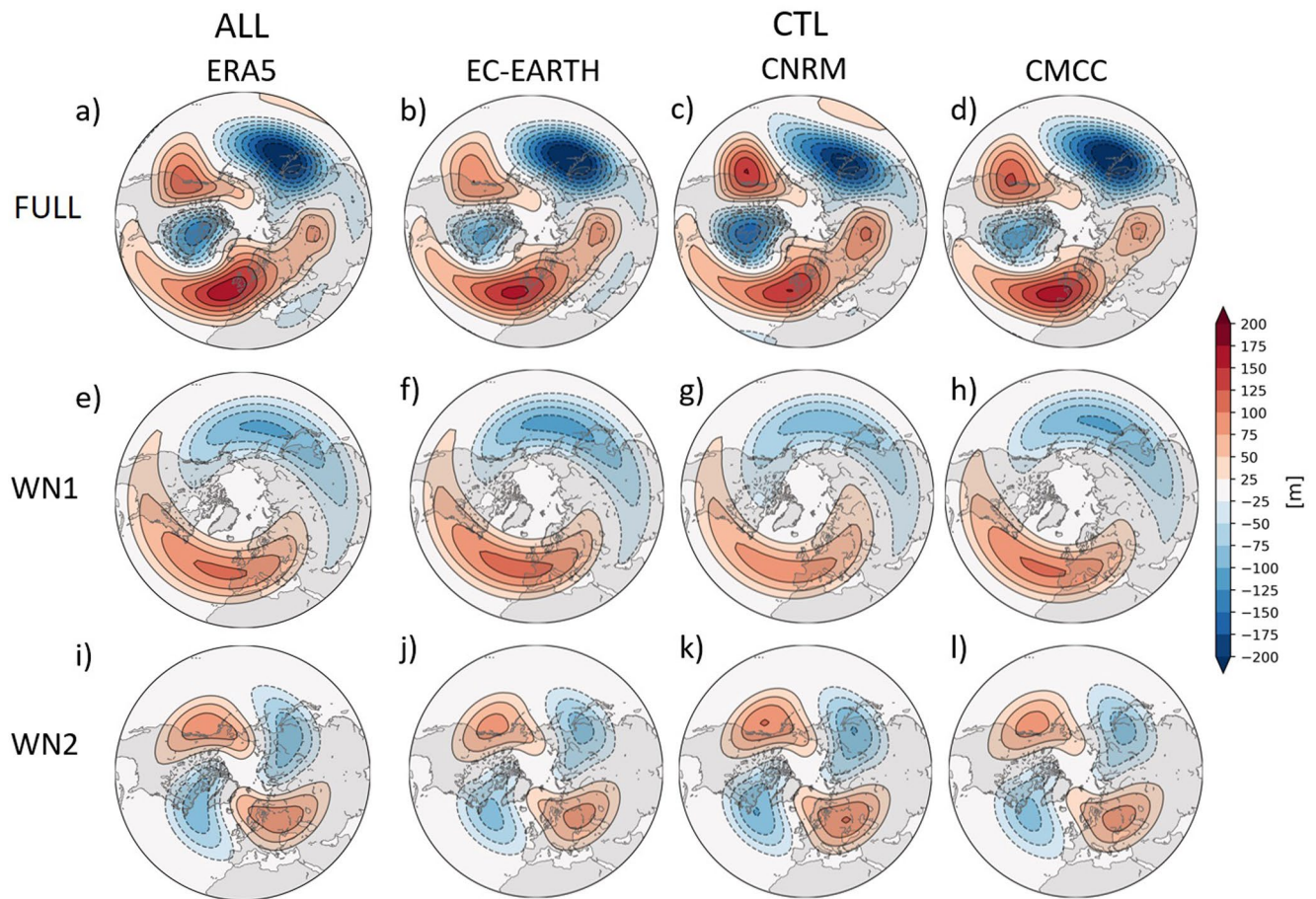
Figure 9. January–February climatological eddy geopotential height at 500 hPa (top) and its wavenumber decomposition into WN1 (middle) and WN2 (bottom) components in (from left to right) ERA5, EC-EARTH, CNRM, and CMCC (CTL experiments).

where the two coincide in sign (Garfinkel et al., 2010), hence likely letting it be more excited than other configurations. This could explain the prevalence of this SSW precursor regardless of ENSO conditions. Further, the eddy heat flux associated with the Eurasian wave pattern (Figure 6) projects onto the climatological centers of positive v^*T^* over central Eurasia and the Aleutian Islands (Newman & Nash, 2000), which are both expected to increase wave injection into the stratosphere before SSWs (e.g., Matsuno, 1971; Polvani & Waugh, 2004).

Despite their similar signal as SSW precursor, a wavenumber decomposition of the Eurasian wave pattern reveals that it is dominated by WN1 for EN whereas WN2 is amplified, becoming comparable to WN1, for LN (Figures 7 and 8). This is consistent with previous studies (Barriopedro & Calvo, 2014; Garfinkel et al., 2012; Song & Son, 2018; Taguchi & Hartmann, 2006) showing the enhancement of WN1 (WN2) before SSWs under EN (LN) conditions. Yet, it is counterintuitive that the same SSW precursor, which in principle is internally generated and so ENSO-unforced, projects onto different wavenumbers depending on the ENSO phase. It is hypothesized here that ENSO modifies the background, stationary wave pattern upon which the SSW-related Eurasian wave pattern superimposes (Figure 10): El Niño (La Niña) leads to a strengthening and anti-clockwise expansion (weakening and clockwise contraction) of the Aleutian Low that favors WN1 (WN2) in the North Pacific; and, by its intrinsic symmetry (namely arithmetically), the wavenumber decomposition of the stationary eddy is affected yielding a reinforcement of WN1 (WN2) over Eurasia. This ENSO modulation of the background wave pattern is robust across models and found in ERA5. Our results outline a framework to understand the potential influence of ENSO on SSW occurrence and, perhaps, to reconcile previous conflicting evidence. Note that it is still not clear why El Niño can dynamically lead to more SSWs while La Niña cannot dynamically lead to less SSWs (Domeisen et al., 2019). Moreover, if the wave driving forced by ENSO were directly responsible for triggering SSWs, why do SSWs not occur every El Niño winter? (e.g., Oehrlein et al., 2019). Our results suggest that the ENSO-forced wavetrain over the North Pacific mainly modulates the
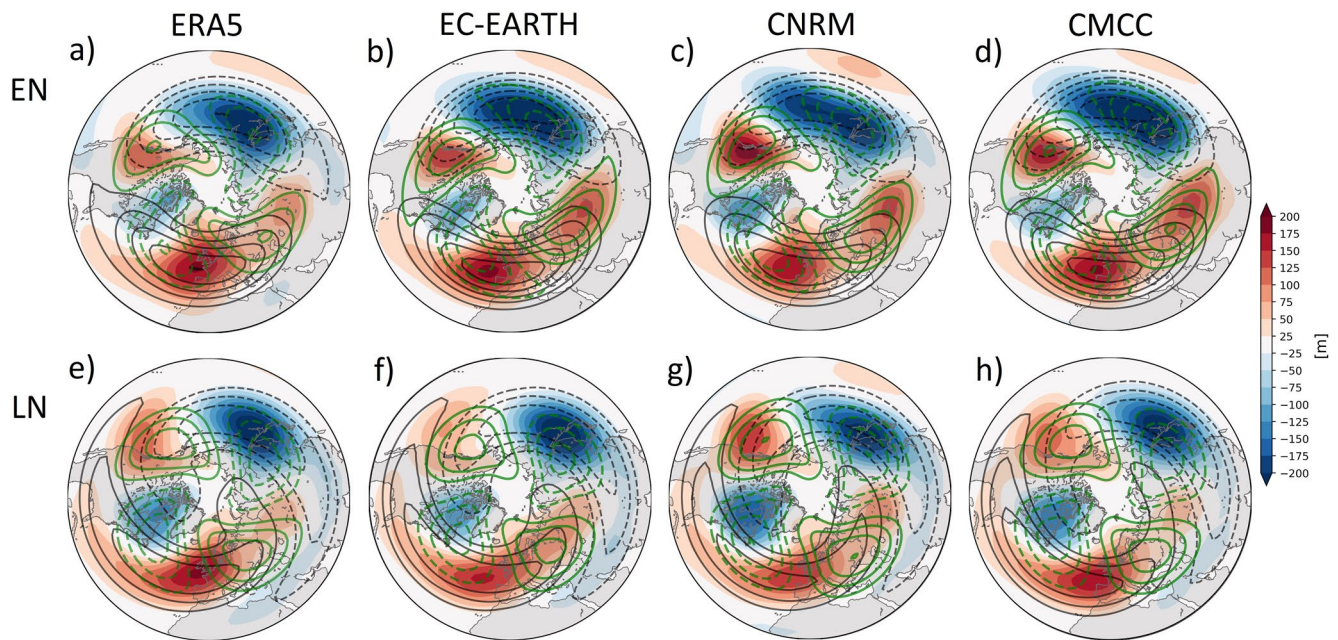
Figure 10. January–February composite-/ensemble-mean eddy geopotential height at 500 hPa for EN (top) and LN (bottom) in (from left to right) ERA5, EC-EARTH, CNRM, and CMCC; WN1 (black contours) and WN2 (green contours) components are superimposed.

seasonal-mean polar vortex, being weaker and more displaced (stronger and more stable) during El Niño (La Niña), particularly in mid-winter/January–February, but it is not the ultimate trigger of the SSWs occurring in those winters. Eventually, the ENSO-unforced wave-like pattern over Eurasia provides the wave injection responsible for those SSWs, with an amplification of WN1 (WN2) for El Niño (La Niña). Note that this framework does not exclude wave driving from other tropospheric precursors (e.g., Garfinkel et al., 2010; Orsolini et al., 2009) or SSWs internally generated in the stratosphere (e.g., Birner & Albers, 2017; de la Cámara et al., 2019). This hypothesis, which might be further assessed, is in line with recent studies (Oehrlein et al., 2019; Polvani et al., 2017) considering that SSWs and ENSO are distinct sources of variability, since in this framework SSWs are essentially not triggered by ENSO and indeed operate at different time-scales, that is, daily weekly the former and monthly seasonally the latter. It is indeed consistent with Garfinkel et al. (2012) who showed that the seasonal-mean stratospheric response to ENSO is largely unrelated to the relative frequency of SSWs during ENSO. Also, in light of these results, and assuming that the temporal variability of the Eurasian wave pattern is unaltered by ENSO, it might be argued that El Niño (La Niña) could increase (decrease) the frequency of SSWs relying on its modulation of the polar vortex strength, as less (more—either bursted or accumulated) wave activity would be needed to trigger SSWs under a weaker (stronger) polar vortex. This is in accordance with the linear ENSO-SSW relationship found in our sensitivity experiments and generally simulated in models (Domeisen et al., 2015; Garfinkel et al., 2012; Polvani et al., 2017; Song & Son, 2018; Taguchi & Hartmann, 2006; Trascasa-Castro et al., 2019), but contrasts with some statistics reported in reanalysis (see Section 1). However, considering the large uncertainty in the observational records and Taguchi and Hartmann's argument that climate modeling can overcome important limitations such as isolating the ENSO forcing and having enough sampling for robustness, it could be argued that the linear ENSO-SSW relationship is dynamically consistent and that some statistics from reanalysis are dominated by internal variability (also in Weinberger et al. (2019); Trascasa-Castro et al. (2019)). This line of research definitely deserves further evaluation. Support to the linear dynamical framework in which ENSO mainly modulates the seasonal-mean state of the polar vortex but it is not directly associated with the precursor of SSWs can be found in Hurwitz et al. (2012) who obtained similar results but for North Pacific SSTs.

Finally, in order to exploit the ENSO-SSW relationship in climate forecasting, particularly in subseasonal-to-seasonal prediction, efforts could be focused on correctly simulating and interpreting the different wave dynamics at play (over the North Pacific and Eurasia) and eddy heat flux in the lower stratosphere, with special attention to its seasonal cycle. Likewise, forecast quality assessment should also try to be dynamics-oriented, going beyond standard skill scores.

Appendix A

The leading variability modes of wave activity over Eurasia are reported and their projection onto the SSW precursors (Figure 5) quantified. NDJFM-daily data over the Eurasian sector 30°E−150°E/20°N–80°N (Bueh & Nakamura, 2007) is considered. The first two leading modes of variability (EOFs) are shown in Figure A1 for all years (ALL) in ERA5 and the control experiment (CTL) in the models. The EOFs for EN and LN experiments are almost identical. Note that these two daily EOFs project on the leading seasonal EOF, namely the Scandinavian/Eurasian wave pattern (not shown).
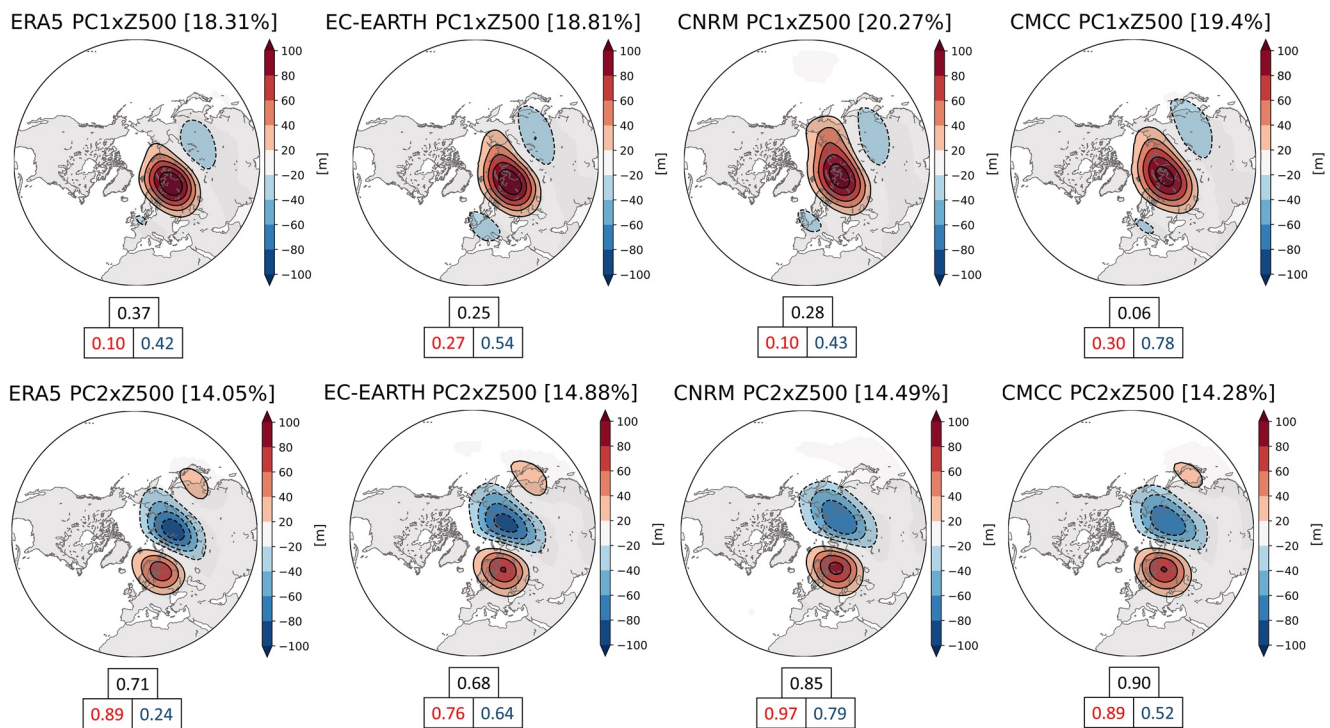

Figure A1. First (top) and second (bottom) leading variability mode of daily geopotential height anomalies at 500 hPa over Eurasia for NDJFM. The fraction of explained variance in each mode is indicated in brackets. Spatial correlations between ALL/CTL (black), EN (red), and LN (blue) SSW precursors (Figure 5) and the EOF patterns are shown.

The similarity between these EOFs and the precursor anomalies of Figure 5 is estimated by the pattern correlation coefficient (numbers in black, red, blue for CTL, EN, LN, respectively). For ALL/CTL, the SSW precursor projects on both EOFs, although dominated by EOF2 with spatial correlations equal or larger than 0.7, except in CMCC for which the contribution of EOF1 is minimal. Interestingly, while for EN the projection of the SSW precursor onto EOF2 is even stronger, for LN the spatial correlation is more equally distributed among EOF1 and EOF2. This result applies to both ERA5 and the models. The distinct spatial projection of the SSW precursors with respect to Eurasian wave activity (EOF1/EOF2) is consistent with the distinct decomposition into wavenumbers reported in the manuscript. Following the modification of the background flow by ENSO (Figure 10), where EN (LN) favors a stronger WN1 (WN2) component: note that the anticyclonic anomaly of EOF2—whose spatial projection is higher for EN—is located more over Scandinavia/western Eurasia, which also has a larger amplitude of WN1 for EN (Figures 10a–10d). On the other hand, for LN, the amplitude of WN1 and WN2 over Eurasia is similar (Figures 10e–10h), and so the spatial projection of the SSW precursor onto EOF1 and EOF2.

Data Availability Statement

References

Ayarzagüena, B., Ineson, S., Dunstone, N. J., Baldwin, M. P., & Scaife, A. A. (2018). Intraseasonal effects of El Niño-Southern oscillation on North Atlantic climate. *Journal of Climate*, *31*(21), 8861–8873. https://doi.org/10.1175/JCLI-D-18-0097.1

Ayarzagüena, B., Palmeiro, F. M., Barriopedro, D., Calvo, N., Langematz, U., & Shibata, K. (2019). On the representation of major stratospheric warmings in reanalyzes. *Atmospheric Chemistry and Physics*, *19*(14), 9469–9484. https://doi.org/10.5194/acp-19-9469-2019

Baldwin, M. P., & Dunkerton, T. J. (2001). Stratospheric harbingers of anomalous weather regimes. *Science*, *294*(5542), 581–584. https://doi.org/10.1126/science.1063315

Barnston, A. G., & Livezey, R. E. (1987). Classification, seasonality and persistence of low-frequency atmospheric circulation patterns. *Monthly Weather Review*, *115*(6), 1083–1126. https://doi.org/10.1175/1520-0493(1987)115<1083:csapol>2.0.co;2

Barriopedro, D., & Calvo, N. (2014). On the relationship between ENSO, stratospheric sudden warmings, and blocking. *Journal of Climate*, *27*(12), 4704–4720. https://doi.org/10.1175/jcli-d-13-00770.1

Bell, B., Hersbach, H., Simmons, A., Berrisford, P., Dahlgren, P., Horányi, A., et al. (2021). The ERA5 global reanalysis: Preliminary extension to 1950. *Quarterly Journal of the Royal Meteorological Society*, *147*(741), 4186–4227. https://doi.org/10.1002/qj.4174

Bell, C. J., Gray, L. J., Charlton-Perez, A. J., Joshi, M. M., & Scaife, A. A. (2009). Stratospheric communication of El Niño teleconnections to European winter. *Journal of Climate*, *22*(15), 4083–4096. https://doi.org/10.1175/2009jcli2717.1

Birner, T., & Albers, J. R. (2017). Sudden stratospheric warmings and anomalous upward wave activity flux. *Sola*, *13*(Special_Edition), 8–12. https://doi.org/10.2151/sola.13a-002

Bladé, I., Newman, M., Alexander, M. A., & Scott, J. D. (2008). The late fall extratropical response to ENSO: Sensitivity to coupling and convection in the tropical West Pacific. *Journal of Climate*, *21*(23), 6101–6118. https://doi.org/10.1175/2008jcli1612.1

Boljka, L., & Birner, T. (2020). Tropopause-level planetary wave source and its role in two-way troposphere–stratosphere coupling. *Weather and Climate Dynamics*, *1*(2), 555–575. https://doi.org/10.5194/wcd-1-555-2020

Bueh, C., & Nakamura, H. (2007). Scandinavian pattern and its climatic impact. *Quarterly Journal of the Royal Meteorological Society: A Journal of the Atmospheric Sciences, Applied Meteorology and Physical Oceanography*, *133*(629), 2117–2131. https://doi.org/10.1002/qj.173

Butler, A. H., & Gerber, E. P. (2018). Optimizing the definition of a sudden stratospheric warming. *Journal of Climate*, *31*(6), 2337–2344. https://doi.org/10.1175/jcli-d-17-0648.1

Butler, A. H., & Polvani, L. M. (2011). El Niño, La Niña, and stratospheric sudden warmings: A reevaluation in light of the observational record. *Geophysical Research Letters*, *38*(13), L13807. https://doi.org/10.1029/2011gl048084

Butler, A. H., Sjoberg, J. P., Seidel, D. J., & Rosenlof, K. H. (2017). A sudden stratospheric warming compendium. *Earth System Science Data*, *9*(1), 63–76. https://doi.org/10.5194/essd-9-63-2017

Cagnazzo, C., & Manzini, E. (2009). Impact of the stratosphere on the winter tropospheric teleconnections between ENSO and the North Atlantic and European region. *Journal of Climate*, *22*(5), 1223–1238. https://doi.org/10.1175/2008jcli2549.1

Cagnazzo, C., Manzini, E., Calvo, N., Douglass, A., Akiyoshi, H., Bekki, S., et al. (2009). Northern winter stratospheric temperature and ozone responses to ENSO inferred from an ensemble of Chemistry Climate Models. *Atmospheric Chemistry and Physics*, *9*(22), 8935–8948. https://doi.org/10.5194/acp-9-8935-2009

Charlton, A. J., & Polvani, L. M. (2007). A new look at stratospheric sudden warmings. Part I: Climatology and modeling benchmarks. *Journal of Climate*, *20*(3), 449–469. https://doi.org/10.1175/jcli3996.1

Charlton-Perez, A. J., Baldwin, M. P., Birner, T., Black, R. X., Butler, A. H., Calvo, N., et al. (2013). On the lack of stratospheric dynamical variability in low-top versions of the CMIP5 models. *Journal of Geophysical Research: Atmospheres*, *118*(6), 2494–2505. https://doi.org/10.1002/jgrd.50125

Cohen, J., & Jones, J. (2011). A new index for more accurate winter predictions. *Geophysical Research Letters*, *38*(21), L21701. https://doi.org/10.1029/2011gl049626

Davini, P., von Hardenberg, J., Corti, S., Christensen, H. M., Juricke, S., Subramanian, A., et al. (2017). Climate SPHINX: Evaluating the impact of resolution and stochastic physics parameterisations in the EC-Earth global climate model. *Geoscientific Model Development*, *10*(3), 1383–1402. https://doi.org/10.5194/gmd-10-1383-2017

de la Cámara, A., Birner, T., & Albers, J. R. (2019). Are sudden stratospheric warmings preceded by anomalous tropospheric wave activity? *Journal of Climate*, *32*(21), 7173–7189. https://doi.org/10.1175/jcli-d-19-0269.1

Deser, C., Simpson, I. R., McKinnon, K. A., & Phillips, A. S. (2017). The Northern Hemisphere extratropical atmospheric circulation response to ENSO: How well do we know it and how do we evaluate models accordingly? *Journal of Climate*, *30*(13), 5059–5082. https://doi.org/10.1175/jcli-d-16-0844.1

Díaz-Durán, A., Serrano, E., Ayarzagüena, B., Abalos, M., & de la Cámara, A. (2017). Intra-seasonal variability of extreme boreal stratospheric polar vortex events and their precursors. *Climate Dynamics*, *49*(9), 3473–3491. https://doi.org/10.1007/s00382-017-3524-1

Domeisen, D. I., Butler, A. H., Fröhlich, K., Bittner, M., Müller, W. A., & Baehr, J. (2015). Seasonal predictability over Europe arising from El Niño and stratospheric variability in the MPI-ESM seasonal prediction system. *Journal of Climate*, *28*(1), 256–271. https://doi.org/10.1175/jcli-d-14-00207.1

Domeisen, D. I., Garfinkel, C. I., & Butler, A. H. (2019). The teleconnection of El Niño Southern Oscillation to the stratosphere. *Reviews of Geophysics*, *57*(1), 5–47. https://doi.org/10.1029/2018rg000596

García-Serrano, J., Frankignoul, C., Gastineau, G., & De La Càmara, A. (2015). On the predictability of the winter Euro-Atlantic climate: Lagged influence of autumn Arctic sea ice. *Journal of Climate*, *28*(13), 5195–5216. https://doi.org/10.1175/jcli-d-14-00472.1

García-Herrera, R., Calvo, N., Garcia, R. R., & Giorgetta, M. A. (2006). Propagation of ENSO temperature signals into the middle atmosphere: A comparison of two general circulation models and ERA-40 reanalysis data. *Journal of Geophysical Research*, *111*(D6), D06101. https://doi.org/10.1029/2005jd006061

García-Serrano, J., Frankignoul, C., King, M. P., Arribas, A., Gao, Y., Guemas, V., et al. (2017). Multi-model assessment of linkages between eastern Arctic sea-ice variability and the Euro-Atlantic atmospheric circulation in current climate. *Climate Dynamics*, *49*(7), 2407–2429. https://doi.org/10.1007/s00382-016-3454-3

Garfinkel, C. I., Butler, A. H., Waugh, D. W., Hurwitz, M. M., & Polvani, L. M. (2012). Why might stratospheric sudden warmings occur with similar frequency in El Niño and La Niña winters? *Journal of Geophysical Research*, *117*(D19), D19106. https://doi.org/10.1029/2012jd017777

Garfinkel, C. I., & Hartmann, D. L. (2007). Effects of the El Niño–Southern Oscillation and the quasi-biennial oscillation on polar temperatures in the stratosphere. *Journal of Geophysical Research*, *112*(D19), D19112. https://doi.org/10.1029/2007jd008481

Garfinkel, C. I., & Hartmann, D. L. (2008). Different ENSO teleconnections and their effects on the stratospheric polar vortex. *Journal of Geophysical Research*, *113*(D18), D18114. https://doi.org/10.1029/2008jd009920

Garfinkel, C. I., Hartmann, D. L., & Sassi, F. (2010). Tropospheric precursors of anomalous Northern Hemisphere stratospheric polar vortices. *Journal of Climate*, *23*(12), 3282–3299. https://doi.org/10.1175/2010jcli3010.1

Hardiman, S. C., Dunstone, N. J., Scaife, A. A., Smith, D. M., Ineson, S., Lim, J., & Fereday, D. (2019). The impact of strong El Niño and La Niña events on the North Atlantic. *Geophysical Research Letters*, *46*(5), 2874–2883. https://doi.org/10.1029/2018gl081776

Hersbach, H., Bell, B., Berrisford, P., Biavati, G., Horányi, A., Muñoz Sabater, J., et al. (2020). ERA5 hourly data on single levels from 1959 to present [Dataset]. Copernicus Climate Change Service (C3S) Climate Data Store (CDS). https://doi.org/10.24381/cds.adbb2d47

Hurwitz, M. M., Newman, P. A., & Garfinkel, C. I. (2012). On the influence of North Pacific sea surface temperature on the Arctic winter climate. *Journal of Geophysical Research*, *117*(D19), D19110. https://doi.org/10.1029/2012jd017819

Ineson, S., & Scaife, A. A. (2009). The role of the stratosphere in the European climate response to El Niño. *Nature Geoscience*, *2*(1), 32–36. https://doi.org/10.1038/ngeo381

Iza, M., Calvo, N., & Manzini, E. (2016). The stratospheric pathway of La Niña. *Journal of Climate*, *29*(24), 8899–8914. https://doi.org/10.1175/jcli-d-16-0230.1

Jiménez-Esteve, B., & Domeisen, D. I. V. (2019). Nonlinearity in the North Pacific atmospheric response to a linear ENSO forcing. *Geophysical Research Letters*, *46*(4), 2271–2281. https://doi.org/10.1029/2018gl081226

King, M. P., Herceg-Bulić, I., Bladé, I., García-Serrano, J., Keenlyside, N., Kucharski, F., et al. (2018). Importance of late fall ENSO teleconnection in the Euro-Atlantic sector. *Bulletin of the American Meteorological Society*, *99*(7), 1337–1343. https://doi.org/10.1175/bams-d-17-0020.1

Kuroda, Y., & Kodera, K. (1999). Role of planetary waves in the stratosphere-troposphere coupled variability in the Northern Hemisphere winter. *Geophysical Research Letters*, *26*(15), 2375–2378. https://doi.org/10.1029/1999gl900507

Limpasuvan, V., Thompson, D. W., & Hartmann, D. L. (2004). The life cycle of the Northern Hemisphere sudden stratospheric warmings. *Journal of Climate*, *17*(13), 2584–2596. https://doi.org/10.1175/1520-0442(2004)017<2584:tlcotn>2.0.co;2

Liu, Y., Wang, L., Zhou, W., & Chen, W. (2014). Three Eurasian teleconnection patterns: Spatial structures, temporal variability, and associated winter climate anomalies. *Climate Dynamics*, *42*(11), 2817–2839. https://doi.org/10.1007/s00382-014-2163-z

Manzini, E., Giorgetta, M. A., Esch, M., Kornblueh, L., & Roeckner, E. (2006). The influence of sea surface temperatures on the northern winter stratosphere: Ensemble simulations with the MAECHAM5 model. *Journal of Climate*, *19*(16), 3863–3881. https://doi.org/10.1175/jcli3826.1

Marshall, A. G., & Scaife, A. A. (2010). Improved predictability of stratospheric sudden warming events in an atmospheric general circulation model with enhanced stratospheric resolution. *Journal of Geophysical Research*, *115*(D16), D16114. https://doi.org/10.1029/2009jd012643

Matsuno, T. (1971). A dynamical model of the stratospheric sudden warming. *Journal of the Atmospheric Sciences*, *28*(8), 1479–1494. https://doi.org/10.1175/1520-0469(1971)028<1479:admots>2.0.co;2

Mezzina, B., Garcia-Serrano, J., Bladé, I., Palmeiro, F. M., Batté, L., Ardilouze, C., et al. (2022). Multi-model assessment of the late-winter extra-tropical response to El Niño and La Niña. *Climate Dynamics*, *58*(7–8), 1965–1986. https://doi.org/10.1007/s00382-020-05415-y

Mezzina, B., Palmeiro, F. M., García-Serrano, J., Bladé, I., Batté, L., & Benassi, M. (2022). Multi-model assessment of the late-winter stratospheric response to El Niño and La Niña. *Climate Dynamics*, *58*(7), 1987–2007. https://doi.org/10.1007/s00382-021-05836-3

Nakagawa, K. I., & Yamazaki, K. (2006). What kind of stratospheric sudden warming propagates to the troposphere? *Geophysical Research Letters*, *33*(4), L04801. https://doi.org/10.1029/2005gl024784

Newman, P. A., & Nash, E. R. (2000). Quantifying the wave driving of the stratosphere. *Journal of Geophysical Research*, *105*(D10), 12485–12497. https://doi.org/10.1029/1999jd901191

Nishii, K., Nakamura, H., & Miyasaka, T. (2009). Modulations in the planetary wave field induced by upward-propagating Rossby wave packets prior to stratospheric sudden warming events: A case-study. *Quarterly Journal of the Royal Meteorological Society: A Journal of the Atmospheric Sciences, Applied Meteorology and Physical Oceanography*, *135*(638), 39–52. https://doi.org/10.1002/qj.359

Oehrlein, J., Chiodo, G., & Polvani, L. M. (2019). Separating and quantifying the distinct impacts of El Niño and sudden stratospheric warmings on North Atlantic and Eurasian wintertime climate. *Atmospheric Science Letters*, *20*(7), e923. https://doi.org/10.1002/asl.923

Orsolini, Y. J., Karpechko, A. Y., & Nikulin, G. (2009). Variability of the Northern Hemisphere polar stratospheric cloud potential: The role of North Pacific disturbances. *Quarterly Journal of the Royal Meteorological Society: A Journal of the Atmospheric Sciences, Applied Meteorology and Physical Oceanography*, *135*(641), 1020–1029. https://doi.org/10.1002/qj.409

Orsolini, Y. J., Kindem, I. T., & Kvamstø, N. G. (2011). On the potential impact of the stratosphere upon seasonal dynamical hindcasts of the North Atlantic Oscillation: A pilot study. *Climate Dynamics*, *36*(3), 579–588. https://doi.org/10.1007/s00382-009-0705-6

Orsolini, Y. J., Kvamstø, N. G., Kindem, I. T., Honda, M., & Nakamura, H. (2008). Influence of the Aleutian-Icelandic low seesaw and ENSO onto the stratosphere in ensemble winter hindcasts. *Journal of the Meteorological Society of Japan Series II*, *86*(5), 817–825. https://doi.org/10.2151/jmsj.86.817

Palmeiro, F. M., Barriopedro, D., García-Herrera, R., & Calvo, N. (2015). Comparing sudden stratospheric warming definitions in reanalysis data. *Journal of Climate*, *28*(17), 6823–6840. https://doi.org/10.1175/jcli-d-15-0004.1

Palmeiro, F. M., García-Serrano, J., Bellprat, O., Bretonnière, P. A., & Doblas-Reyes, F. J. (2020). Boreal winter stratospheric variability in EC-EARTH: High-Top versus Low-Top. *Climate Dynamics*, *54*(5), 3135–3150. https://doi.org/10.1007/s00382-020-05162-0

Peings, Y. (2019). Ural blocking as a driver of early-winter stratospheric warmings. *Geophysical Research Letters*, *46*(10), 5460–5468. https://doi.org/10.1029/2019gl082097

Polvani, L. M., Sun, L., Butler, A. H., Richter, J. H., & Deser, C. (2017). Distinguishing stratospheric sudden warmings from ENSO as key drivers of wintertime climate variability over the North Atlantic and Eurasia. *Journal of Climate*, *30*(6), 1959–1969. https://doi.org/10.1175/jcli-d-16-0277.1

Polvani, L. M., & Waugh, D. W. (2004). Upward wave activity flux as a precursor to extreme stratospheric events and subsequent anomalous surface weather regimes. *Journal of Climate*, *17*(18), 3548–3554. https://doi.org/10.1175/1520-0442(2004)017<3548:uwafaa>2.0.co;2

Portal, A., Ruggieri, P., Palmeiro, F. M., García-Serrano, J., Domeisen, D. I., & Gualdi, S. (2022). Seasonal prediction of the boreal winter stratosphere. *Climate Dynamics*, *58*(7), 2109–2130. https://doi.org/10.1007/s00382-021-05787-9

Roehrig, R., Beau, I., Saint-Martin, D., Alias, A., Decharme, B., Guérémy, J. F., et al. (2020). The CNRM global atmosphere model ARPEGE-Climat 6.3: Description and evaluation. *Journal of Advances in Modeling Earth Systems*, *12*(7), e2020MS002075. https://doi.org/10.1029/2020ms002075

Ruggieri, P., Buizza, R., & Visconti, G. (2016). On the link between Barents-Kara sea ice variability and European blocking. *Journal of Geophysical Research: Atmospheres*, *121*(10), 5664–5679. https://doi.org/10.1002/2015jd024021

Ruggieri, P., Kucharski, F., Buizza, R., & Ambaum, M. H. P. (2017). The transient atmospheric response to a reduction of sea-ice cover in the Barents and Kara Seas. *Quarterly Journal of the Royal Meteorological Society*, *143*(704), 1632–1640. https://doi.org/10.1002/qj.3034

Sanna, A., Borrelli, A., & Athanasiadis, P. (2017). *The CMCC seasonal prediction system*. CMCC Research Paper.285.

Sassi, F., Kinnison, D., Boville, B. A., Garcia, R. R., & Roble, R. (2004). Effect of El Niño–Southern Oscillation on the dynamical, thermal, and chemical structure of the middle atmosphere. *Journal of Geophysical Research*, *109*(D17), D17108. https://doi.org/10.1029/2003jd004434

Song, K., & Son, S. W. (2018). Revisiting the ENSO–SSW relationship. *Journal of Climate*, *31*(6), 2133–2143. https://doi.org/10.1175/jcli-d-17-0078.1

Taguchi, M., & Hartmann, D. L. (2006). Increased occurrence of stratospheric sudden warmings during El Niño as simulated by WACCM. *Journal of Climate*, *19*(3), 324–332. https://doi.org/10.1175/jcli3655.1

Takaya, K., & Nakamura, H. (2008). Precursory changes in planetary wave activity for midwinter surface pressure anomalies over the Arctic. *Journal of the Meteorological Society of Japan Series II*, *86*(3), 415–427. https://doi.org/10.2151/jmsj.86.415

Timmermann, A., An, S. I., Kug, J. S., Jin, F. F., Cai, W., Capotondi, A., et al. (2018). El Niño–southern oscillation complexity. *Nature*, *559*(7715), 535–545. https://doi.org/10.1038/s41586-018-0252-6

Titchner, H. A., & Rayner, N. A. (2014). The Met Office Hadley Centre sea ice and sea surface temperature data set, version 2: 1. Sea ice concentrations. *Journal of Geophysical Research: Atmospheres*, *119*(6), 2864–2889. https://doi.org/10.1002/2013jd020316

Toniazzo, T., & Scaife, A. A. (2006). The influence of ENSO on winter North Atlantic climate. *Geophysical Research Letters*, *33*(24), L24704. https://doi.org/10.1029/2006gl027881

Trascasa-Castro, P., Maycock, A. C., Yiu, Y. Y. S., & Fletcher, J. K. (2019). On the linearity of the stratospheric and Euro-Atlantic sector response to ENSO. *Journal of Climate*, *32*(19), 6607–6626. https://doi.org/10.1175/jcli-d-18-0746.1

Trenberth, K. E., Branstator, G. W., Karoly, D., Kumar, A., Lau, N. C., & Ropelewski, C. (1998). Progress during TOGA in understanding and modeling global teleconnections associated with tropical sea surface temperatures. *Journal of Geophysical Research*, *103*(C7), 14291–14324. https://doi.org/10.1029/97jc01444

Van Loon, H., & Labitzke, K. (1987). The Southern Oscillation. Part V: The anomalies in the lower stratosphere of the Northern Hemisphere in winter and a comparison with the quasi-biennial oscillation. *Monthly Weather Review*, *115*(2), 357–369. https://doi.org/10.1175/1520-0493(1987)115<0357:tsopvt>2.0.co;2

Voldoire, A., Saint-Martin, D., Sénési, S., Decharme, B., Alias, A., Chevallier, M., et al. (2019). Evaluation of CMIP6 deck experiments with CNRM-CM6-1. *Journal of Advances in Modeling Earth Systems*, *11*(7), 2177–2213. https://doi.org/10.1029/2019ms001683

Weinberger, I., Garfinkel, C. I., White, I. P., & Oman, L. D. (2019). The salience of nonlinearities in the boreal winter response to ENSO: Arctic stratosphere and Europe. *Climate Dynamics*, *53*(7), 4591–4610. https://doi.org/10.1007/s00382-019-04805-1

Erratum

In the originally published version of this article, in Table 1, the thirty-second row of the first column contained a typographical error. The years "1981/19182" should be "1981/1982." The error has been corrected, and this may be considered the authoritative version of record.